ELSEVIER

Chemical Engineering Journal 93 (2003) 81–90

Chemical Engineering Journal

www.elsevier.com/locate/cej

Mesoporous platinum as a catalyst for oxygen electroreduction and methanol electrooxidation

Anthony Kucernak*, Junhua Jiang

Department of Chemistry, Imperial College of Science, Technology and Medicine, South Kensington, London SW7 2AZ, UK

Abstract

A mesoporous platinum catalyst (H_I-Pt) containing pores of diameter 34 Å has been examined as a potential catalytic material for both the electrochemical reduction of oxygen and the electrochemical oxidation of methanol. The material has been characterized in sulfuric acid at room temperature by voltammetry and chronoamperometry as an abrasively deposited microelectrode. About one-quarter of the internal pore surface area appears to be electrochemically accessible.

The material shows good activity towards the reduction of dissolved dioxygen molecules, with an exchange current density and Tafel slope close to that seen for conventional dispersed platinum catalysts.

The mass activity towards the oxygen reduction in 0.5 mol dm^{-3} H_2SO_4 reaction is quite low, at 1.1 A g^{-1}, and the specific activity is also quite low at 7.4 μA cm^{-2}, both at 900 mV (RHE). Both these low values may be due to the relatively poor surface area to volume ratio of this particular catalyst formulation.

In comparison, the methanol oxidation activity seems to be significantly improved compared to normal dispersed platinum catalysts in 0.5 mol dm^{-3} H_2SO_4 and 1 mol dm^{-3} CH_3OH with values of 20 A g^{-1}, and 42 mA cm^{-2} at 0.55 V (RHE) and 65 °C. A discussion of the unique features of this catalyst and how the structural morphology of the mesoporous phase may affect the electrocatalytic activity of the catalyst is given.

Keywords: Platinum; Electrocatalyst; Fuel cell; Oxygen reduction reaction; Methanol oxidation reaction

1. Introduction

Highly dispersed high surface area catalysts are used in many heterogeneous catalytic and electrocatalytic processes. Such materials are highly important to phosphoric acid and solid polymer electrolyte fuel cells (PAFC and SPEFC, respectively). In such fuel cells the catalyst is primarily used in the form of platinum and platinum alloy colloidal particles, which are either supported or unsupported. Fuel cells pose a distinct set of challenges over and above those commonly seen within normal heterogeneous catalysis. These problems derive from the necessity of providing optimum ionic and electronic conductivity and reactant/product transport at the catalyst surface.

Electrons produced at the cathode and consumed at the anode must be collected and efficiently distributed to the other electrode. This necessitates utilizing a support that is electrically conductive, but which at the same time must be resistant towards corrosion in the extreme electrochemical environment in the fuel cell.

Cations must flow from the anode to the cathode (H_3O^+, as is the case for the PAFC and SPEFC), or from the cathode to the anode (OH^-, CO_3^{2-}, or O^{2-} for the alkaline, carbonate and solid oxide fuel cells, respectively). Thus it is necessary to provide a suitable ionically conducting medium between the anode and the cathode. The ionic conductors used within fuel cells are typically much less conductive than electronic conductors—for instance, the conductivity of Nafion, a commonly used proton conducting material in SPEFCs is 0.083 S cm^{-1} [1], whereas the conductivity of carbon is 1375 S cm^{-1} [2]. Thus it is advantageous to keep the separation between the anode and cathode within the fuel cell as small as possible, as this reduces resistive losses, which would tend to occur in the membrane.

The net result is that for efficient operation of PAFCs or SPEFCs the catalyst layer is required to be thin and to be composed of either unsupported or supported catalyst at high loading (typically 10–40 wt.% loading). This constraint provides an extra challenge to the design of fuel cell electrodes, and drives the need to discover methods of producing high loading, highly dispersed catalysts which can be fashioned into very thin catalyst layers—typically of the order of 10 μm.

* Corresponding author. Tel.: +44-20-7594-5831; fax: +44-20-7594-5804.
E-mail address: a.kucernak@ic.ac.uk (A. Kucernak).

1385-8947/02/$ – see front matter © 2002 Elsevier Science B.V. All rights reserved.
PII: S1385-8947(02)00111-0

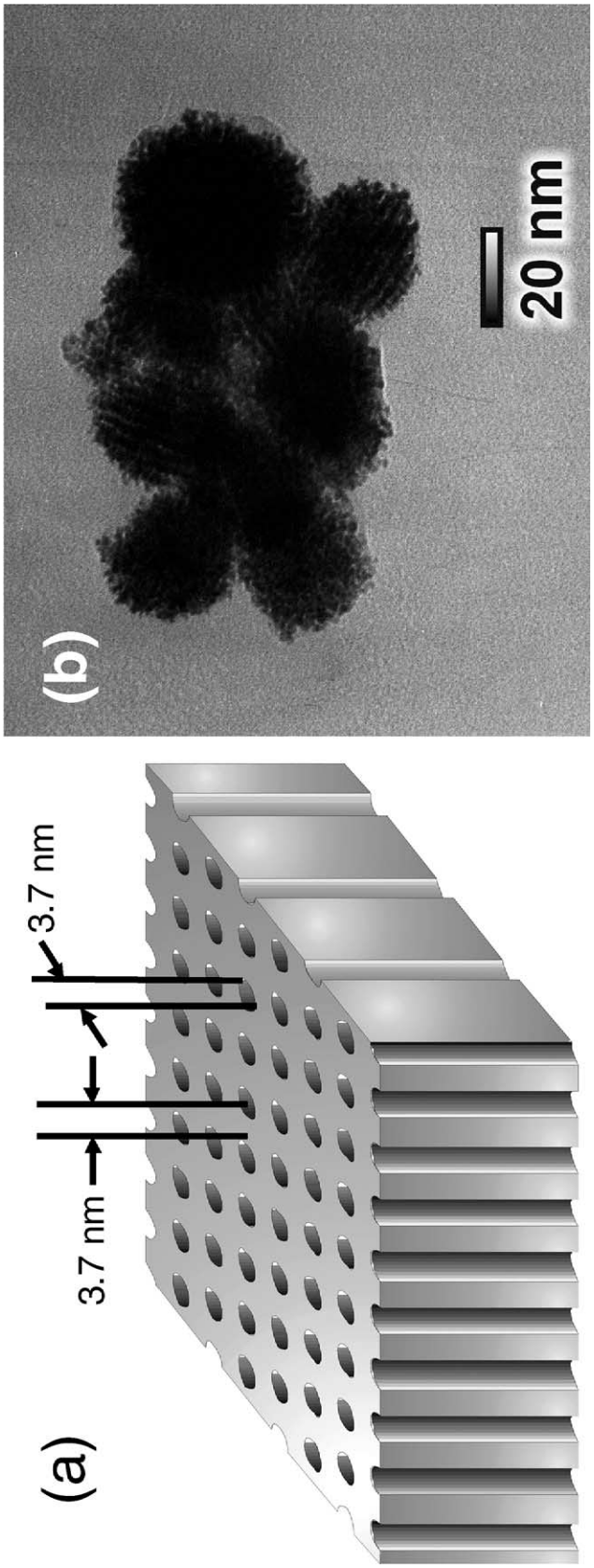

Fig. 1. (a) Schematic diagram of the geometry of the mesoporous H_I-platinum catalyst; (b) TEM image of one particle of the mesoporous H_I-platinum catalyst.

As previously mentioned, the catalyst of choice is supported or unsupported precious metal particles of small diameter, typically less than 10 nm, with a lower limit of about 1 nm. If supported, a graphitic carbon is often used, as carbon is one of the few inexpensive electrically conductive materials that are stable in the electrochemical environment of the fuel cell. The intrinsic activity of these catalysts (i.e. the activity per unit area) is found to be quite dependent upon particle diameter.

As an alternative, several approaches may be used to produce a high surface area monolithic catalytic layer. For instance, relatively large-scale mesoporous metal films with porosity in the range 200–1000 nm have been produced utilizing silica or polystyrene spheres as templates [3].

On a finer scale, there has been considerable research into the production of ordered mesoporous materials (i.e. materials with pores in the 2–50 nm range) through directed templating techniques [4,5]. Initial work concentrated on the production of metal oxides with well-defined pore sizes [6,7]. This approach has been significantly broadened by the introduction of liquid crystal templating materials, as reviewed by Raimondi and Seddon [8]. Such an approach has been used by Attard et al. [9,10] to produce a range of mesoporous metallic systems.

Porous platinum films have been produced through either chemical or electrochemical reduction of a system composed of a lyotropic liquid crystal within which dihydrogen hexachloroplatinic acid (HCP) is dissolved in the aqueous phase [11,12]. Such porous platinum films have roughness factors of over 200 [12], and are composed of film or particles which typically contain a regular array of cylindrical pores of 1–10 nm in diameter separated by walls of the same thickness [13] as illustrated in the cartoon in Fig. 1a. Furthermore, it has been suggested that these materials would make ideal catalysts for fuel cell systems [14].

In this paper, we present a study of the activity towards the oxygen reduction and methanol oxidation reactions of mesoporous platinum material, H_I-Pt, produced from the hexagonal phase of the non-ionic surfactant octaethylene glycol monohexadecyl ether ($C_{16}E_8$-$CH_3(CH_2)_{15}O(CH(CH_2OH))_7CH_2CH_2OH$). A TEM of our catalytic material is presented in Fig. 1b. Although such catalysts have been electrodeposited onto a microelectrode to examine their activity for oxygen reduction [15], our approach is unique in allowing us to obtain the activity and performance of a 'real-world' catalyst, produced through chemical reduction means and deposited in a quick and reproducible way on an electrode [16].

2. Experimental

2.1. Chemicals

Sulfuric acid solutions were prepared using deionised water (18 MΩ cm conductance, Millipore MilliQ system), and AnalaR grade reagent. Solutions were deoxygenated with high purity argon. Mesoporous platinum metal was synthesized by reduction of H_2PtCl_6 dissolved in the normal topology hexagonal phase of a non-ionic surfactant at 40 °C [11]. The material is porous with hexagonally spaced parallel pores 3.4 nm in diameter separated by 3.4 nm platinum walls. The material was found to have a surface area of 47 $m^2\ g^{-1}$ by N_2 BET, slightly larger than that calculated from purely geometric arguments. Analysis of similar samples to those used here using both TEM and X-ray diffraction shows the well-defined mesoporous structure of this catalyst [17].

2.2. Preparation of the electrodes

Cha et al. [18] developed a simple technique for the investigation of powder electroactive substances and analyzed its basic electrochemical behavior. Such an approach has also recently used an electrode prepared by mechanical abrasion to investigate the electrochemistry of insoluble and unconductive microcrystals [19]. The abrasively deposited microelectrode was prepared as follows. A small amount of the mesoporous platinum powdery was placed on a smooth glass plate. The end of a gold microdisk electrode was heavily rubbed on the H_I-Pt. Successful deposition of the H_I-Pt was evidenced by the silver-white color of the microdisk. The abrasion process does not appear to destroy the mesoporous structure of the H_I-Pt.

2.3. Electrochemical measurements

Voltammetric measurements were performed at room temperature (20 °C) using an Autolab General Purpose Electrochemical System (Ecochemie, Netherlands). A three-compartment cell with Luggin capillary for the reference arm and a glass frit between the counter electrode compartment and the main cell was used for the majority of experiments. The counter electrode was a Pt flag and the reference electrode was a saturated calomel electrode (SCE). Potentials were corrected to the RHE potential scale.

3. Results

3.1. Characterization of microelectrodes

The abrasion process will inevitably produce a deposited layer of larger surface area than that of the underlying microelectrode, Fig. 2. This layer may be characterized by an apparent radius, r', greater than the radius of the underlying microelectrode, r. It is also characterized by film thickness, x, which ideally is very much smaller than r' to eliminate the possibility of concentration polarization within the film. Ideally, r' should be less than 2–3 times greater than r, as resistive losses in the film, especially for small values of x

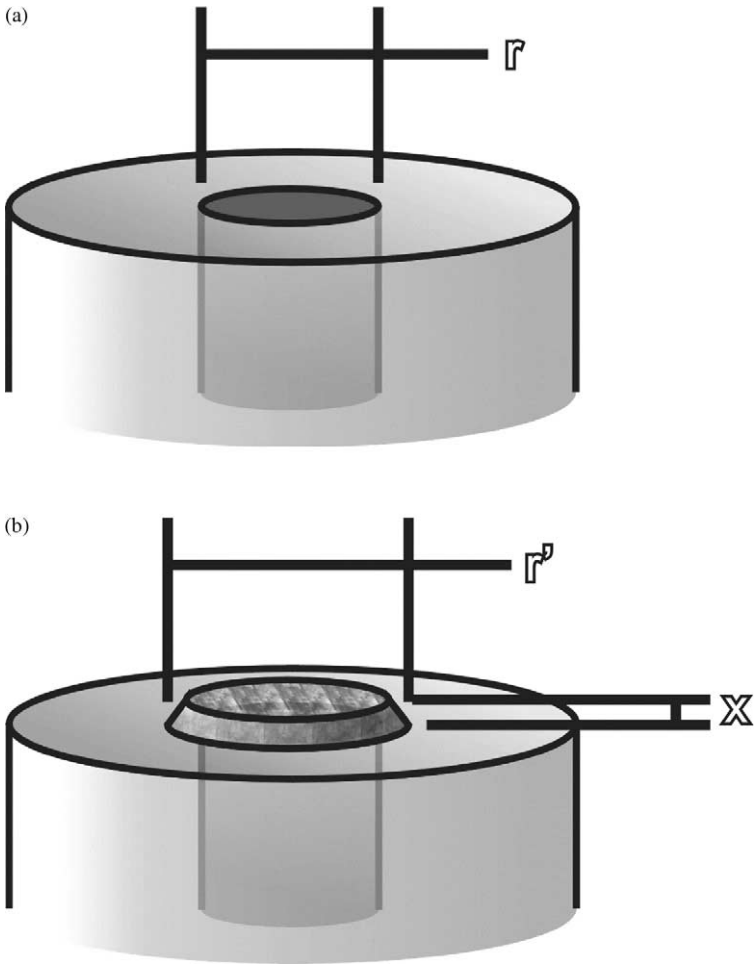

Fig. 2. Comparison between a normal microelectrode (a) and an electrode with an abrasively deposited layer on its surface (b). In the case of the latter, the effective radius of the deposit r' will be greater or equal to the radius of the underlying microelectrode, r. The deposit will also have a finite thickness, x.

may cause distortion in the electrochemical response of the system. As the amount of material deposited on the electrode is not known, it is necessary to experimentally determine the loading, and the effective radius of the electrode, r'. This is achieved by measurement of both the total surface area of the electrode (i.e. including the internal surface area), and the projected surface area.

Fig. 3 shows the voltammogram of a H_I-Pt rubbed microelectrode in 0.5 mol dm^{-3} H_2SO_4 solution. Current is expressed in terms of the projected surface area, as determined below. The features in the hydrogen adsorption/desorption region can be rationalized on the basis of hydrogen electrochemistry on platinum low-index single-crystal surfaces in acid solutions [20].

The real surface area of the H_I-Pt may be estimated from the hydrogen adsorption/desorption charge, Q_H, in the potential region between 0 and 0.4 V, assuming a monolayer of hydrogen corresponds to an adsorption charge of 210 μC cm^{-2} [21]. The hydrogen adsorption charge can be determined via $2Q_H = (Q_{total} - Q_{dl})$, represented by the shaded area in Fig. 3, where Q_{total} is the total charge transferred in the hydrogen adsorption/desorption and Q_{dl} the capacitative charge due to double-layer charging, as measured from the current in the double-layer region.

The average diameter of the rubbed layer was determined from the diffusion-limited current due to the reduction

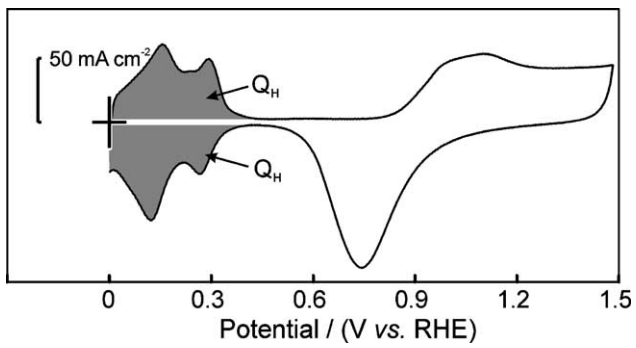

Fig. 3. Cyclic voltammogram for a rubbed H_I-Pt microelectrode in 0.5 mol dm^{-3} H_2SO_4 at a scan rate of 0.20 V s^{-1}.

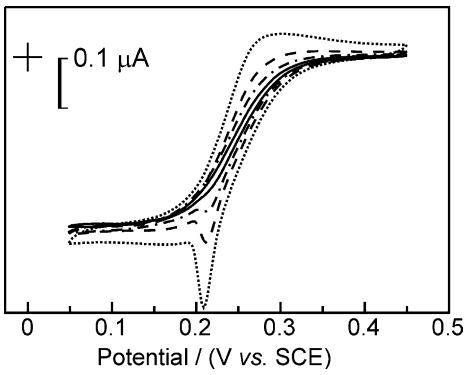

Fig. 4. Cyclic voltammogram for a rubbed H_I-Pt microelectrode in 0.020 mol dm^{-3} $K_3Fe(CN)_6$ + 1 mol dm^{-3} KCl as a function of scan rate: 2 mV s^{-1} (—); 5 mV s^{-1} (—·—·—); 10 mV s^{-1} (— — —) and 20 mV s^{-1} (···).

of potassium hexacyanoferrate(III) ($K_3Fe(CN)_6$). As the reduction of $Fe(CN)_6^{3-}$ is kinetically facile, all of the $Fe(CN)_6^{3-}$ which reaches the surface of the electrode will be reduced, and none will have a chance to diffuse into the porous material. Thus the steady-state behavior of the powder microelectrode is the same as that of a planar microdisk electrode with the same diameter [18]. The generally accepted equation for the steady-state diffusion-limited current at a planar microdisk is as follows:

$$I_d = 4nFDcr_0 \quad (1)$$

where n is the number of electrons transferred during the electrochemical reaction, F the Faraday's constant, D and c are, respectively, the diffusion coefficient and concentration of the electroactive species, and r_0 the radius of the disk.

The equation above is only adhered to at steady-state, and there may be deviations from it if the system undergoes some dynamic transient. Displayed in Fig. 4 are the cyclic voltammograms for the reduction of a solution composed of 0.020 mol dm^{-3} $K_3Fe(CN)_6$ + 1 mol dm^{-3} KCl as a function of scan rate. Two effects are significant in these voltammograms. The first observation is that at faster scan rates there is an obvious peak formed during the reduction process before a limiting current is obtained. This peak decreases in magnitude as the scan rate decreases, and is not present at sufficiently slow scan rates. The second observation is that the limiting current at faster scan rates is larger than those obtained at slower scan rates. The formation of peaks in the voltammograms at microelectrodes has been ascribed to the changeover from planar to hemispherical diffusion geometry, and this process has been modeled by Aoki et al. [22].

Thus in order to ensure that only the exposed geometric surface, and not the internal surface area, is active for the $Fe(CN)_6^{3-}$ reduction, it is necessary to scan at sufficiently slow sweep rates and utilize sufficiently dilute $Fe(CN)_6^{3-}$ solution. Thus we have utilized a sweep rate of 0.5 mV s^{-1} and a $Fe(CN)_6^{3-}$ concentration of 0.02 mol dm^{-3}.

The diffusion coefficient of $Fe(CN)_6^{3-}$ has been determined as being 7.63 × 10^{-6} cm^2 s^{-1} [23], with n = 1 in a solution composed of 0.020 mol dm^{-3} $K_3Fe(CN)_6$ + 1 mol dm^{-3} KCl we obtain a value for effective diameter of the deposited layer of 116 μm. The mass of deposited material was estimated from the electrochemical surface area, and the known specific surface area measured using the BET method. In separate experiments, production of Nafion bound electrodes of known loading led to electrochemical measurement of only 26% of the BET area, and so we correct for this discrepancy. We presume that this discrepancy is due to incomplete wetting of the porous structure or due to subtle differences in the two surface measurement processes. Nonetheless, during our electrochemical reactions we saw no variation in the electrochemical surface area, implying that the surface area and roughness factors which we have measured are time-invariant.

The roughness factor, R_F, the ratio of the real surface area to the geometric surface area, is calculated as 360. This is a very high value—much larger than that of a usual planar electrode or even electrodeposited electrode. This fact confirms the well-developed surface area of this mesoporous material.

The mass of H_I-Pt on the microelectrode is about 2.4 × 10^{-7} g, i.e. a loading of about 2.4 mg cm^{-2}. So it is possible to estimate the film thickness of the rubbed layer

$$L = \frac{m}{V_{H_I\text{-Pt}}\rho A_0} \quad (2)$$

where m is the mass of rubbed layer, $V_{H_I\text{-Pt}}$ the volume fraction of platinum in the material (0.61), ρ the platinum density (21.4 g cm^{-3}) and A_0 the geometric surface area of the rubbed layer. The film thickness was found to be about 2 μm, which implies that our electrodes may be considered as a powder microelectrode with a very thin active layer.

3.2. Oxygen reduction reaction

Fig. 5 shows a steady-state polarization curve for the H_I-Pt rubbed microelectrode in O_2-saturated 0.5 mol dm^{-3} H_2SO_4. In comparison to the previous experiments involving $Fe(CN)_6^{3-}$, oxygen is reduced at a much slower rate and thus it is expected that oxygen will tend to diffuse through the entire structure of the porous material, and not just be reduced at the external interface of the electrode. A well-developed limiting current plateau I_d can clearly be seen. The concentration and diffusion coefficient of dissolved oxygen in 0.5 mol dm^{-3} H_2SO_4 solution have been reported as being 1.13 × 10^{-6} mol cm^{-3} and 1.8 × 10^{-5} cm^2 s^{-1}, respectively [24]. Cha et al. [18] investigated oxygen reduction on acetylene-black-packed microelectrode in KOH solution and found the same Tafel slopes on carbon powder microelectrode and planar carbon

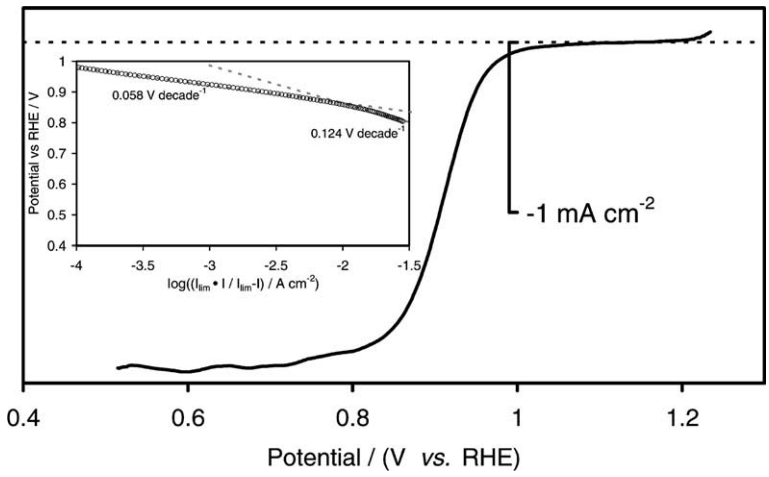

Fig. 5. Steady-state polarization curve for dissolved oxygen on rubbed H_I-Pt microelectrode in 0.5 mol dm^{-3} H_2SO_4, saturated with pure oxygen. $\nu = 0.1$ mV s^{-1}. Inset: Tafel plot for this curve.

electrodes. They concluded that the porous electrocatalysts in the powder microelectrode is homogeneously polarized and the powder microelectrode is equivalent to a planar electrode with an enhanced surface area. If the film thickness of the rubbed microelectrode is limited to some few microns it is reasonable to assume that polarization within the porous electrode is homogeneous. For our experiment on the H_I-Pt electrode, and utilizing Eq. (1), the electron number is calculated to be 4.4 per oxygen molecule, a little larger the theoretical value of 4.

Data points from the kinetically controlled regions of the steady-state curve were chosen for Tafel analysis. These data are corrected for mass-transport effects by calculating the parameter $i_d i/(i_d - i)$, where i is the current density at a given potential and i_d the limiting current density. The Tafel plot of such data is shown in the inset of Fig. 5. The plot shows two well-defined linear regions extending over three orders of magnitude in current density. These regions have slopes of 58 and 124 mV per decade. A value for the exchange current densities, i_0, may be obtained by extrapolation of the Tafel line to the equilibrium potential, E_{eq}, for the O_2 reduction (1.23 V vs. RHE). The exchange current density for O_2 reduction on the H_I-Pt corresponding to each Tafel slope is shown in Table 1.

Typically, performance of oxygen reduction catalysts are reported as mass activities or specific activities at 0.9 V (RHE). In Table 2 we present the mass and specific activities for the oxygen reduction reaction at this potential using the rubbed microelectrode.

Table 2
Mass and specific activities of H_I-platinum to the oxygen reduction reaction measured at 0.9 V vs. RHE in 0.5 mol dm^{-3} H_2SO_4

	Mass activity at 900 mV (RHE) (A g^{-1} Pt)	Specific activity at 900 mV (RHE) (μA cm^{-2})
H_I-Pt microelectrode	1.1	7.4

3.3. Methanol oxidation reaction

Platinum has been long recognized as an effective methanol oxidation catalyst, and it shows exceptionally high initial activity [25,26]. Unfortunately, although it shows high activity for short times, it quickly deactivates due to the adsorption of carbon monoxide intermediates on its surface [27,28]. Alloying platinum with ruthenium overcomes the poisoning problem to some extent, and leads to catalysts which show reasonably stable activity. Unfortunately, activity is still hindered to a certain extent by the build-up of CO on the catalyst surface [29,30]. Although a mesoporous *PtRu* material of the type reported in this paper has been synthesized, this material has not been tested for methanol

Table 1
Tafel slope (b) and exchange current density (i_0) for oxygen reduction at an H_I-platinum in 0.5 mol dm^{-3} H_2SO_4[a]

Electrode	Low current density		High current density		Reference
	b (V per decade)	i_0 (A cm^{-2})	b (V per decade)	i_0 (A cm^{-2})	
H_I-Pt microelectrode	0.058	4.9×10^{-9}	0.124	1.11×10^{-5}	This work
Pt disk microelectrode	0.063	2.0×10^{-9}	0.119	7.8×10^{-7}	[27]

[a] Nafion electrolyte.

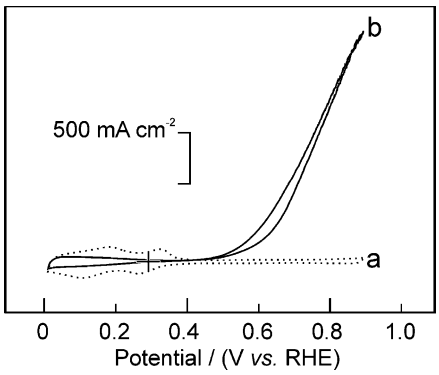

Fig. 6. Cyclic voltammogram at a temperature of 60 °C of a rubbed H_I-Pt microelectrode in 0.5 mol dm^{-3} H_2SO_4 (a) and 0.5 mol dm^{-3} H_2SO_4 + 0.5 mol dm^{-3} CH_3OH (b). For both voltammograms the scan rate is 50 mV s^{-1}.

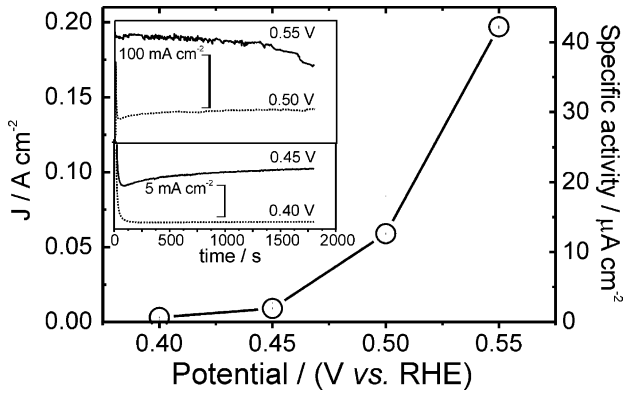

Fig. 7. Pseudo steady-state activity of a rubbed H_I-Pt microelectrode in 0.5 mol dm^{-3} H_2SO_4 + 0.5 mol dm^{-3} CH_3OH, at a temperature of 60 °C. Left axis shows activity in terms of projected surface area, and right axis shows activity in terms of real surface area. Inset: chronoamperograms of the response of the current as a function of applied potential. Electrode loading of 10 mg cm^{-2} Pt.

oxidation activity although it does show good activity for heterogeneous CO oxidation [17]. As no experiments have been performed on methanol oxidation using this new mesoporous material, we have looked at the oxidation of methanol on our H_I-Pt microelectrodes.

Presented in Fig. 6 are voltammograms for a H_I-Pt microelectrodes in 0.5 mol dm^{-3} H_2SO_4 in the presence and absence of methanol at a temperature of 60 °C. The current is normalized to the geometrical surface area of the electrode. The loading of platinum on the electrode was calculated to be 10 mg cm^{-2}, with an average thickness of 7 μm. Such a thin layer will be homogeneously polarized under the conditions of study.

It can be seen that the electrode manages to sustain very high activities for the methanol oxidation process, especially at higher potentials. The specific activity (i.e. current divided by real surface area) of the catalyst is higher than those typically seen on either polycrystalline platinum or on nanoparticulate systems under similar conditions [31].

As discussed previously, one of the principle disadvantages of platinum as a catalyst for methanol oxidation is that the activity quickly decays with time. Thus, although the voltammogram, Fig. 6, suggests a highly active catalyst, the results only prove that the instantaneous rates of methanol oxidation are high. In order to obtain more conclusive results of the activity of the H_I-Pt mesoporous catalysts activity towards methanol oxidation, we have used chronoamperometry to look at the time variation of the oxidation rate of methanol on the catalyst.

Fig. 7 shows the steady-state polarization plot for the H_I-Pt microelectrode in 0.5 mol dm^{-3} H_2SO_4 + 0.5 mol dm^{-3} CH_3OH at a temperature of 60 °C. The data were acquired after the electrode had been polarized for 1000 s. It can be seen that especially at high potentials, the catalyst is able to sustain high oxidation rates for some time. Inset of this figure shows the chronoamperograms for the electrode at different potentials. At all potentials, the activity is initially quite high, but it decreases quite markedly over the first 100–200 s. At the lowest potential displayed, 0.40 V, the current remains stable after this initial period. At higher potentials, 0.45 and 0.5 V, after the initial deactivation there follows a period during which the current again increases, partially offsetting the initial drop—this reactivation of the electrode is not normally seen for the oxidation of methanol on platinum at either room temperature or at 60 °C [32]. At still higher potentials, 0.55 V, the current trace appears much more noisy, with sudden jumps in the current. Over longer periods there is a decrease in the magnitude of the current. The noise spikes were correlated with bubbles forming at the surface of the microelectrode, and it is believed that the decrease in the magnitude of the current is due to the formation of a stationary bubble on the surface of the electrode which hindered mass transport of methanol to the electrode surface. There is also some possibility that the vigorous agitation caused by bubble formation lead to loss of some of the catalyst from the surface of the microelectrode. It is not believed that the long-term loss in current is due to poisoning of the electrode by carbonaceous intermediates, as such effects tend to be much less significant at higher potentials [32].

4. Discussion

For very high dispersions, that is for small particle sizes, typical platinum and platinum alloy catalysts exhibit a cubooctahedral geometry [33]. As the degree of dispersion is increased, the ratio of the different facets available for the electrocatalytic reaction to occur on will change, and this may very well be the reason for the well-documented catalyst-size effect seen for both the methanol oxidation reaction [31,34] and for the oxygen reduction reaction [35,36].

One of the most interesting aspects of the H_I-Pt mesoporous catalysts is that it has a strong negative surface

curvature compared to normal nanodispersed platinum catalysts, which have a positive surface curvature. This also means that the crystal faces making up the surface of the catalyst will be significantly different from those for normal cubooctahedral catalysts, although the actual mix of different crystal faces present in these catalysts have not been measured. Because of the significant differences in activity for both oxygen reduction [37] and methanol oxidation [38] on different crystal faces, and the expected differences of faces present in the H_I-Pt catalyst, we might very well expect different activities for different electrocatalytic reactions.

4.1. Oxygen reduction reaction

A comparison between the Tafel slopes and calculated exchange current densities in both the high current and low current regions for the H_I-Pt catalyst and for pure E-Tek platinum for the O_2 reduction reaction is displayed in Table 1. The data for the latter was taken from the work of Perez et al. [39].

A Tafel plot showing two linear segments with slopes of about RT/F (∼60 mV per decade) and $2RT/F$ (∼120 mV per decade) have usually been reported for the O_2 reduction reaction on platinum electrode in acidic medium and at the platinum/Nafion interface [40]. These variations in the Tafel slopes are attributed to the influence of different adsorption and different rate-determining steps over the potential ranges investigated [40]. As displayed in Table 1, the Tafel slopes and exchange current densities calculated for our H_I-Pt catalyst are quite similar to the values determined for a typical high surface area dispersed catalysts [39]. Such values are quite typical of both supported or unsupported platinum, suggesting that in the H_I-Pt catalyst there is no significant effect of the platinum morphology on the mechanism of oxygen reduction.

Birkin et al. [15] measured voltammograms for oxygen reduction on high surface area H_I-Pt electrodes in air-saturated pH 7 phosphate buffer. The electrodes were produced through an electrodeposition process, which allowed easy control of the thickness of the deposited layer. Although no analysis of the kinetic parameters for oxygen reduction on these electrodes are given, the electron number of the oxygen reduction reaction at high roughness factors is seen to be 4.4, the same as the value that we obtain. The determination of electron number made an implicit assumption that the solubility and diffusion coefficient of molecular oxygen within the pores of the mesoporous material was the same as that in the bulk solution. Transport in mesoporous and nanoporous media is highly complex, and diffusion coefficients as well as viscosities within such materials are liable to be different from those found in bulk solution, and thus may, in principle, explain the discrepancy in the calculated electron number [41].

The mass activity and specific area activity to the reduction of dissolved oxygen have been extensively investigated using thin film platinum and carbon-supported platinum in different media [42,43]. The size of the platinum particle has been found to have an obvious effects on the electrocatalytic oxygen reduction activity. The reported values are experimentally dependent. Most investigations have shown that platinum with a particle size of 3–4 nm can provide a peak mass activity ranging from 1.4 to 25 A g^{-1} and a peak specific activity ranging from 1 to 70 μA cm^{-2} both measured at 0.9 V vs. RHE [9,42,43]. The mass and specific activities for the H_I-Pt used in our study are presented in Table 2.

The mass activity of our material at 1–2 A g^{-1} at 900 mV (RHE) is towards the low end of the range listed above. This can be attributed to the relatively low surface area to volume ratio of this catalyst when compared to optimum-sized platinum particles. In fact, for the catalyst used here, the surface area to volume ratio is the same as for platinum particles with a diameter of about 20 nm, which is large compared to the normal size of catalysts utilized for oxygen reduction. As mentioned above, it also appears as if we can only access about one-fourth of the surface area of the platinum, as judged by H-adsorption/desorption. Were we able to access all of the internal pore area, the surface area to volume ratio would improve, producing a value equivalent to platinum particles of 8 nm diameter.

Poirier and Stoner found that mass activity and specific activity at 0.9 V vs. RHE both decrease with increasing particle size (and decreasing specific surface area). A TEM investigation of our catalyst, Fig. 1, shows a particle size of about 20–40 nm, although the material is composed of many inner pores of about diameter 3.4 nm separated by walls with a thickness of 3.4 nm. The utilization of inner pores dramatically increases the mass and specific activity, although not enough to offer better performance when compared to current catalysts.

4.2. Methanol oxidation reaction

Mass and specific activities of H_I-platinum to the methanol oxidation reaction compared to values obtained in the literature under the same conditions are presented in Table 3. The mass activity for methanol oxidation is quite high when compared to other data in the literature, especially considering that this data is for supported catalysts, which typically show higher activity than unsupported catalysts [31,44,45]. In comparison, the specific activity of the catalyst does not seem to be significantly different from that obtained on planar platinum electrodes. This apparent contradiction may be rationalized by the significant effect which particle size has on the activity of dispersed catalysts towards the methanol electrooxidation reaction. Indeed, the results suggest that were the surface area to volume ratio of the H_I-platinum catalyst improved (by moving to a system with smaller pores and smaller pore separation), it may be possible to significantly surpass the methanol oxidation activities currently seen for dispersed platinum catalysts.

Table 3
Mass and specific activities of H_I-platinum to the methanol oxidation reaction measured at 0.55 V vs. RHE in 0.5 mol dm^{-3} H_2SO_4 and 0.5 mol dm^{-3} CH_3OH at 60 °C

	Mass activity at 550 mV (RHE) (A g^{-1} Pt)	Specific activity at 550 mV (RHE) (μA cm^{-2})	Reference
10 mg cm^{-2} H_I-Pt microelectrode	20	42	This work
Smooth platinum	–	49	[32]
5 mg cm^{-2} ~20 wt.% Pt/C	15	–	[44]
1 mg cm^{-2} 10 wt.% Pt/C	10	–	[45]

The improved activity seen for methanol oxidation on the H_I-platinum catalyst may be due to a number of contributory factors. Work is on going in our laboratory to understand the precise mechanism behind the apparent increase in activity towards methanol oxidation, although it seems likely that the process may be due to one of the following mechanisms:

(a) improved water activation on the H_I-platinum surface;
(b) higher surface ratio of platinum crystallographic orientations advantageous to methanol oxidation; or
(c) the acceleration on the H_I-platinum of a parallel pathway which results in a decrease in the formation of the surface species, presumably adsorbed CO, responsible for deactivation of the platinum electrocatalyst.

Water activation is an important process in the oxidation of the adsorbed intermediates formed during the oxidation of methanol [31]. Were the mesoporous H_I-platinum more likely to adsorb water than normal dispersed platinum, for instance, due to the negative surface curvature present within the pores of the material, then it might be expected that an improvement in methanol oxidation activity would be observed. Alternatively, it has already been shown that the rate of methanol oxidation is critically dependent upon the crystallographic orientation of the underlying facet, with differences of two orders of magnitude on different the facets present in highly dispersed catalysts observed [46]. It might very well be expected that the geometry of the mesoporous H_I-platinum necessitate a different ratio of crystallographic planes. Thus a different activity would be observed for the methanol oxidation reaction. Finally, there is strong evidence that the methanol oxidation reaction follows parallel pathways one of which does not involve the production of adsorbed CO [47]. Were this secondary pathway accelerated relative to the 'normal' pathway, then a decrease in poisoning sensitivity and increase in activity may very well be expected.

Although the activity of the H_I-platinum catalyst is still significantly less than that obtained on alloy catalysts, it is nonetheless intriguing that this catalyst shows higher activity and does not appear to suffer from the significant deactivation seen on normal highly dispersed platinum particles. Such unusual activity suggests that a templated mesoporous alloy catalysts (e.g. composed of Pt/Ru) may offer a fruitful area to explore in order to produce new and more active methanol oxidation catalysts.

Acknowledgements

This project has been funded by the United Kingdom EPSRC and MOD/DERA under Grant GR/L 57920.

References

[1] T.E. Springer, T.A. Zawodzinski, S. Gottesfeld, J. Electrochem. Soc. 138 (1991) 2334.
[2] R.C. Weast (Ed.), Handbook of Chemistry and Physics, 61st ed., CRC Press, 1980, F-173.
[3] K.M. Kulinowski, P. Jiang, H. Vaswani, V.L. Colvin, Adv. Mat. 12 (2000) 833.
[4] U. Ciesla, F. Schuth, Micropor. Mesopor. Mater. 27 (1999) 131.
[5] D.Y. Zhao, P.D. Yang, Q.S. Huo, B.F. Chmelka, G.D. Stucky, Curr. Opin. Solid State Mater. Sci. 3 (1998) 111.
[6] P.T. Tanev, T.J. Pinnavaia, Science 267 (1995) 865.
[7] D.M. Antonelli, J.Y. Ying, Chem. Mater. 8 (1996) 874.
[8] M.E. Raimondi, J.M. Seddon, Liq. Cryst. 26 (1999) 305.
[9] G.S. Attard, C.G. Goltner, J.M. Corker, S. Henke, R.H. Templer, Angew. Chem. Int. Edit. 36 (1997) 1315.
[10] G.S. Attard, N.R.B. Coleman, J.M. Elliott, Stud. Surf. Sci. Catal. 117 (1998) 89.
[11] G.S. Attard, P.N. Bartlett, N.R.B. Coleman, J.M. Elliott, J.R. Owen, J.H. Wang, Science 278 (1997) 838.
[12] J.M. Elliott, P.R. Birkin, P.N. Bartlett, G.S. Attard, Langmuir 15 (1999) 7411.
[13] J.M. Elliott, G.S. Attard, P.N. Bartlett, N.R.B. Coleman, D.A.S. Merckel, J.R. Owen, Chem. Mater. 11 (1999) 3602.
[14] J.M. Elliott, G.S. Attard, P.N. Bartlett, J.R. Owen, N. Ryan, G. Singh, J. New Mater. Electrochem. Syst. 2 (1999) 239.
[15] P.R. Birkin, J.M. Elliott, Y.E. Watson, Chem. Commun. 1693 (2000).
[16] J.J. Jiang, A. Kucernak, Electrochem. Solid State Lett. 3 (2000) 559.
[17] G.S. Attard, S.A.A. Leclerc, S. Maniguet, A.E. Russell, I. Nandhakumar, P.N. Bartlett, Chem. Mater. 13 (2001) 1444.
[18] C.S. Cha, C.M. Li, H.X. Yang, P.F. Liu, J. Electroanal. Chem. 368 (1994) 47.
[19] A.M. Bond, S. Fletcher, P.G. Symons, Analyst 123 (1998) 1891.
[20] N.M. Marković, B.N. Grgur, P.N. Ross, J. Phys. Chem. B 101 (1997) 5405.
[21] T. Biegler, D.A.J. Rand, R. Woods, J. Electroanal. Chem. 29 (1971) 269.
[22] K. Aoki, K. Akimoto, K. Tokuda, H. Matsuda, J. Osteryoung, J. Electroanal. Chem. 171 (1984) 219.
[23] J. Koryta, J. Dvořák, L. Kavan, Principles of Electrochemistry, second ed., Wiley, Chichester, UK, 1993.
[24] S. Gottesfeld, I.D. Raistrick, S. Srinivasan, J. Electrochem. Soc. 134 (1987) 1455.
[25] E. Herrero, K. Franaszczuk, A. Wieckowski, J. Phys. Chem. 98 (1994) 5074.
[26] T.D. Jarvi, S. Sriramulu, E.M. Stuve, J. Phys. Chem. B 101 (1997) 3649.

[27] R. Parsons, T. Vandernoot, J. Electroanal. Chem. 257 (1988) 9.
[28] T.D. Jarvi, E.M. Stuve, Fundamental aspects of vacuum and electrocatalytic reactions of methanol and formic acid on platinum surfaces, in: J. Lipkowski, P.N. Ross (Eds.), Electrocatalysts, Wiley/VCH, New York/Weinheim, 1998, p. 75.
[29] H.N. Dinh, X. Ren, F.H. Garzon, P. Zelenay, S. Gottesfeld, J. Electroanal. Chem. 491 (2000) 222.
[30] G.T. Burstein, C.J. Barnett, A.R. Kucernak, K.R. Williams, Catal. Today 38 (1997) 425.
[31] T. Frelink, W. Visscher, J.A.R. Vanveen, J. Electroanal. Chem. 382 (1995) 65.
[32] H.A. Gasteiger, N. Markovic, P.N. Ross, E.J. Cairns, J. Electrochem. Soc. 141 (1994) 1795.
[33] N. Giordano, E. Passalacqua, L. Pino, A.S. Arico, V. Antonucci, M. Vivaldi, K. Kinoshita, Electrochim. Acta 36 (1991) 1979.
[34] F. Gloaguen, J.M. Leger, C. Lamy, J. Appl. Electrochem. 27 (1997) 1052.
[35] A. Gamez, D. Richard, P. Gallezot, F. Gloaguen, R. Faure, R. Durand, Electrochim. Acta 41 (1996) 307.
[36] Y. Takasu, N. Ohashi, X.G. Zhang, Y. Murakami, H. Minagawa, S. Sato, K. Yahikozawa, Electrochim. Acta 41 (1996) 2595.
[37] N. Markovic, H. Gasteiger, P.N. Ross, J. Electrochem. Soc. 144 (1997) 1591.
[38] A. Crown, H. Kim, G.Q. Lu, I.R. de Moraes, C. Rice, A. Wieckowski, J. New Mater. Electrochem. Syst. 3 (2000) 275.
[39] J. Perez, E.R. Gonzalez, E.A. Ticianelli, Electrochim. Acta 44 (1998) 1329.
[40] A. Parthasarathy, C.R. Martin, S. Srinivasan, J. Electrochem. Soc. 138 (1991) 916.
[41] D. Nicholson, K. Travis, in: N.K. Kanellopoulos (Ed.), Recent Advances in Gas Separation by Microporous Ceramic Membranes, Vol. 257, Elsevier, Amsterdam, 2000.
[42] J.A. Poirier, G.E. Stoner, J. Electrochem. Soc. 141 (1994) 425.
[43] M. Peuckert, T. Yoneda, R.A.D. Betta, M. Boudart, J. Electrochem. Soc. 133 (1986) 944.
[44] A. Hamnett, S.A. Weeks, B.J. Kennedy, G. Troughton, P.A. Christensen, Ber. Bunsenges. Phys. Chem. 94 (1990) 1014.
[45] W. Zidong, G. Hetong, T. Zhiyuan, J. Power Source 58 (1996) 239.
[46] V. Radmilovic, H.A. Gasteiger, P.N. Ross, J. Catal. 154 (1995) 98.
[47] S. Sriramulu, T.D. Jarvi, E.M. Stuve, Electrochim. Acta 44 (1998) 1127.